Photoinduced electric effects in various plasmonic materials

David Keene[1], Paula Fortuno[1], Natalia Noginova[1], Maxim Durach[2]

[1]Center for Materials Research, Norfolk State University, Norfolk, VA USA
[2]Department of Physics, Georgia Southern University, Statesboro, GA USA

Received xxxxxx
Accepted for publication xxxxxx
Published xxxxxx

Abstract

Photoinduced voltages associated with surface plasmon polariton excitations are studied both theoretically and experimentally in various plasmonic systems as the function of material, wavelength, and type of structure. Experimental photovoltage normalized to the absorbed power shows a general decrease upon an increase in the wavelength, enhancement in the nanostructured samples, and a strong variation in the magnitude as a function of the material, which are not in line with the theoretical predictions of the simple plasmonic pressure approach. The results can be used for clarification of the mechanisms and further development of an adequate theoretcial approach to the plasmon drag effect.

Keywords: Plasmon, Plasmon Drag Effect, Photocurrent

Introduction

Strongly confined and greatly enhanced light fields at the nanoscale present a new playground for fundamental studies as they lead to new or enhanced phenomena associated with the interaction of light and matter. Understanding the mechanisms of such effects is important for both fundamental physics and applications [1-14]. Significant DC electrical effects, electric potentials, and photocurrents associated with plasmonic excitations [15-32] are among these effects. Electric potentials reported in [21] show different signs for illumination at wavelengths below or above the localized surface plasmon resonance (LSP) and are explained with a thermodynamic approach [22]. The plasmon drag effect (PLDE) [15-19, 24, 25] involves directionality, and is commonly discussed in terms of momentum transfer from plasmons to electrons [26, 27]. The polarity of the electrical signals commonly corresponds to a drag of the electrons in the direction of SPP propagation. The photoinduced electric currents are greatly enhanced in nanostructured systems [18, 23] where they are sensitive to nanoscale geometry [18], light polarization (linear, or left//right circular light polarization [20]) and can be directed parallel or antiparallel to plasmon polariton propagation [23, 24, 31]. They also show a strong sensitivity to surface modification [25].

The electromagnetic hydrodynamic momentum loss approach [26, 27] predicts effective forces acting in the plasmonic metal: plasmonic pressure (analogous to light pressure) and plasmonic striction (equivalent to a pondermotive force). This theory provides a good qualitative description for the plasmon drag effect in flat films and profile-modulated systems with a relatively low amplitude of the profile modulation [23]. However, it predicts the signal amplitudes significantly lower than those observed in experiment and needs additional assumptions to explain the photovoltage magnitudes [27]. Later, it was found in various experiments, that the plasmonic pressure mechanism does not provide a full explanation of several experimental findings, such as a sharp switching in the polarity of photocurrents in profile-modulated films with a high profile-modulation height

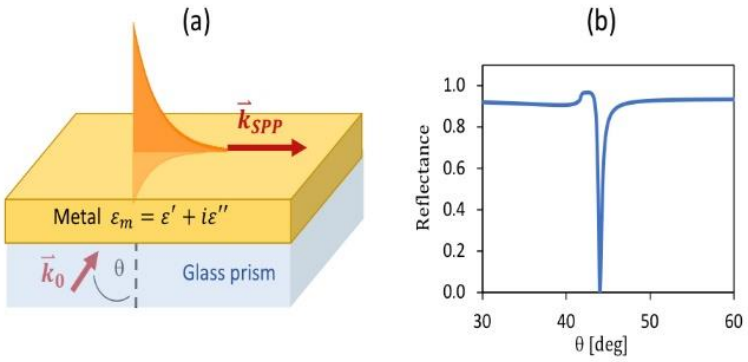

Figure 1. (a) Excitation of the SPP in Kretschmann geometry; (b) Angular dependence of reflectivity in assumption of perfect coupling.

upon a small variation in the incidence angle [24], or polarity switching in flat films when pumping air out of the chamber containing the film [30]. The effects of surface morphology [24,31], surface charges [30], or the nonlinearity of electron motion [18, 28] are suggested in literature as important factors, which may play an additional or, possibly, a major role in the effect.

More experimental studies are needed to better understand the mechanisms contributing to PLDE, for validation of the current approach or development of a new one. Previous experiments mostly target the angular dependence of the effect and are performed at one wavelength of illumination. Gold or silver are common metals used. In this study, we explore various materials, obtain the spectral dependences of photoinduced electrical signals, and compare the effects in flat and nanostructured systems. First, we theoretically estimate the effective forces acting in our materials based on the momentum loss approach [26], then perform the experimental studies and discuss the obtained results in comparison with the theoretical predictions.

Method

1.1 Theoretical estimations

In the electromagnetic hydrodynamic momentum loss approach [26], the Lorentz force $\bar{f}_{L_i}$ acting on electrons in plasmonic fields can be presented as a sum of two terms, the effective plasmonic striction, f_s, and plasmonic pressure, f_p, as

$$\bar{f}_{L_i} = f_s + f_p = \frac{1}{2} Re\{\chi\} \cdot Re\{E_\alpha \partial_i E_\alpha^*\} - \frac{1}{2} Im\{\chi\} \cdot Im\{E_\alpha \partial_i E_\alpha^*\}, \quad (1)$$

where a and i are x, y, and z and χ is the complex susceptibility of a plasmonic material. Let us consider various materials where plasmonic excitations can take place, such as gold, silver, aluminum, copper, platinum, permalloy, and titanium nitride (TiN), and estimate the effective forces as functions of the wavelength in each material under consideration. In the estimations, we use the data for the dielectric permittivities of metals (bulk values) from the database [34]; the laser pulse is assumed to have an energy of 1 mJ, a duration of 10 ns and, illuminate the area 3 mm wide and 4 mm long.

For simplicity, we consider a flat film geometry, which corresponds to the experimental situation depicted in figure 1. The SPP is excited in a strip of thin metal film with p-polarized light in the Kretschmann geometry. In calculations, we assume a perfect (critical) coupling of the incident wave and SPP with the maximum depth of the reflection dip. From the solutions of Maxwell's equations at the metal-dielectric interface, the SPP wave-vector, skin depths of the field penetration into the metal, δ_m, and the dielectric, δ_d, and the energy of the SPP per unit area, $\mathcal{E}_{SPP}$, can be found as

$$k_{spp} = k_0 \left(\frac{\epsilon'_m \epsilon_d}{\epsilon'_m + \epsilon_d} \right)^{\frac{1}{2}} + i\, k_0 \frac{\epsilon''_m}{2\epsilon'^2_m} \left(\frac{\epsilon'_m \epsilon_d}{\epsilon'_m + \epsilon_d} \right)^{\frac{3}{2}}$$

$$\delta_m = \frac{1}{k_0} \left(\frac{|\epsilon'_m| + \epsilon_d}{\epsilon'^2_m} \right)^{\frac{1}{2}} \quad (2)$$

$$\delta_d = \frac{1}{k_0} \left(\frac{|\epsilon'_m| + \epsilon_d}{\epsilon'^2_d} \right)^{\frac{1}{2}}$$

$$\mathcal{E}_{SPP} = \frac{P}{2k'' v_g},$$

where $k_0 = \frac{\omega}{c}$. and $v_g = \frac{1}{\frac{dk_{SPP}}{d\omega}}$. Here P is the intensity of the incident beam, ω is the frequency and c is the speed of light.

The plasmonic pressure force, $f_p = -\frac{1}{2} Im\{\chi\} \cdot Im\{E_\alpha \partial_i E_\alpha^*\}$ is related to the linear momentum transfer from SPPs to

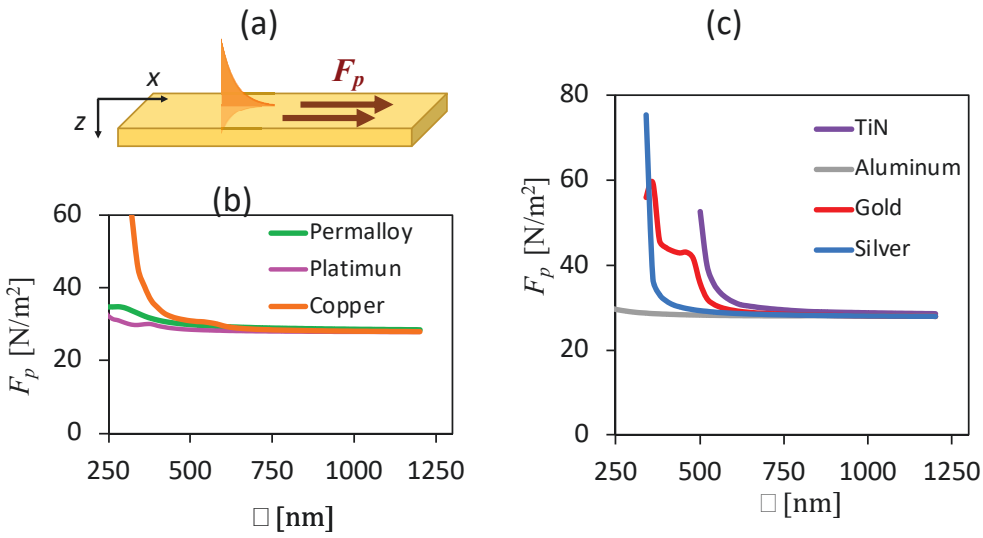

Figure 2. (a) Pressure force acting in the surface layer in the direction of the SPP propagation; (b) and (c) Estimations for different materials (indicated with color).

electrons and is determined by the SPP momentum and the rate of SPP absorption which takes place in the skin-layer [27, 29]. In flat geometry, the total plasmonic pressure acting on the electrons in the plasmonic film per unit surface area can be found as

$$F_p = \frac{P}{\hbar\omega}\,\hbar k_{SPP} = \frac{P}{c}\left(\frac{\epsilon'_m \epsilon_d}{\epsilon'_m + \epsilon_d}\right)^{1/2}. \qquad (3)$$

Estimations for the materials under consideration (assuming the parameters of illumination described above and a metal-air interface) are shown in figure. 2.

As one can see, if that pressure force is the underlying mechanism for PLDE, the spectral behaviour of the effect in each material should be nearly the same: the wavelength dependence is weak for most of the optical and near infra-red range. A rapid increase in the signal is expected with a decrease in the wavelength due to the growth of the SPP wavevector and the corresponding momentum. For estimating the photoinduced voltages, additional considerations need to be taken into account, including the parameters of the electrical circuits in the measurements and the momentum relaxation time which can vary from material to material. This is discussed below in the Experimental section.

The striction force pushes electrons from bright spots (opposite to the action of the pondermotive force in laser tweezers, since χ_m is negative in metals). Assuming relatively slow changes in light intensity across the illuminated spot (along the *x*-axis), and a DC regime for the electric circuit, it acts perpendicular to the surface, with the volume density determined by the gradient of the light intensity [26] as

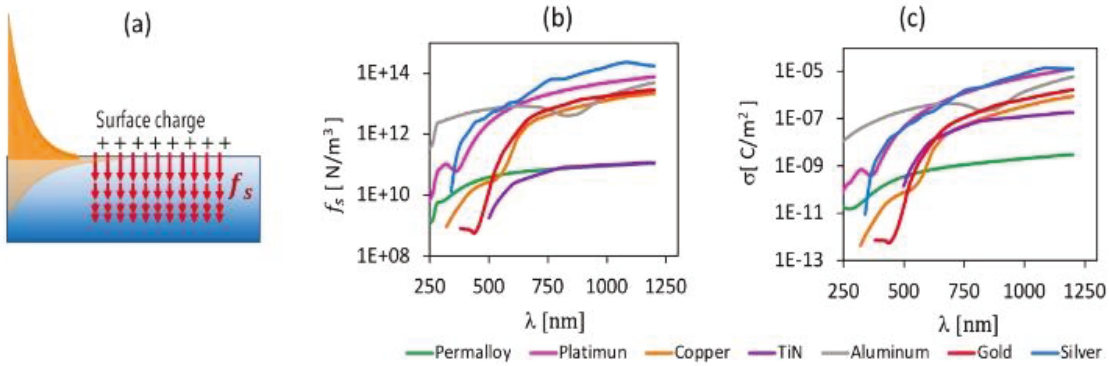

Figure 3. (a) Direction of the effective stiction force in a flat geometry; (b) Striction force f_s and (c) surface charge σ in various materials indicated with color.

$$f_s = \chi_m \epsilon_0 \frac{d(E^2)}{dz} = \frac{2\chi_m}{\delta_m} E_0^2 e^{2z/\delta_m} = \chi_m \frac{4\mathcal{E}_{SPP}}{\epsilon'_m \delta_m^2} e^{\frac{2z}{\delta_m}} \quad (4)$$

where χ_m is the real part of the metal dielectric susceptibility. It decreases the free electron concentration, *n,* by Δn near the interface and induces a surface charge, σ, which can be estimated as

$$\Delta n = \frac{8\,\epsilon'_m \epsilon_0}{n\,\delta_m^3 e^2}\mathcal{E}_{SPP}, \qquad \sigma = \frac{e\Delta n \delta_m}{2} = \frac{4\epsilon_0\,\epsilon'_m}{n\,\delta_m^2 e}\mathcal{E}_{SPP}\,. \quad (5)$$

Our predictions for different materials are shown in Fig. 3. The wavelength dependence is the opposite of the plasmonic pressure force: it increases with an increase in the wavelength. It plays a role in transient signals at ultrashort pulse illumination [26]. In an ideal situation of perfectly flat geometry in the closed-circuit DC regime, this force should not contribute to the voltage across the sample. However, in nanostructures, it may generate voltages across individual nanofearures in the case of nonlinear or ballistic electron flow [18]. If the striction force is the major driving force in a particular experiment, one should expect a large difference in the effect from one metal to the other and an increase in the effect magnitude upon increase in the wavelength of illumination.

2.2 Experiment

In the experiments, we use two types of samples, flat films (our primary subject of study) and profile-modulated systems fabricated using various metals, see Table 1. Most of the deposition (Gold, Silver, Copper, Aluminum) is done in a conventional thermal evaporation system; Plasma Sputtering is used for Platinum; and Permalloy (Py) is deposited through e-Beam evaporation. For the prisms, we use a mask to produce a thin film in the shape of a 3 mm wide strip 15 mm long (the approximate width of the prism). Flat films are deposited onto the large face of high-index prisms (N SF-11 Schott glass right angle prisms) (Fig. 4 (a)). The profile-modulated systems are fabricated from commercially available DVD-R disks from Verbatim™. The disks are forcibly delaminated and separated into two. The read/write polycarbonate side, which is originally covered with a photo-reactive material, serves as the basis for our samples. The photo-reactive layer is washed out with methanol and the substrate is dried with Nitrogen. A 3 mm wide radial strip is cut from the disc. The substrate has a square-wave profile (see Fig. 4 (b)) with a period of 740 nm and an amplitude of about 100-120 nm. The actively monitored portion of the sample, the area between the electrical contacts, is 15 mm in length mirroring the flat films described above.

	Flat films on prisms					Gratings		
Material	Ag	Au	Pt	Al	Cu	Ag	Au	Py
Thickness $d \pm 1$ [nm]	35	35	35	34	40	30	35	40
Resistance [Ω]	3.5	5.3	84.3	30	86	80	130	180

Table 1. Materials and parameters of the experimental samples

The thicknesses of the produced samples, *d*, (Table 1) are estimated with profilometer measurements on witness samples of glass substrate produced during the same deposition run. Since the parameters of the electrical circuit play a role in the observed photovoltage, we also measure the resistances with a 4-point contact technique. The resistances are higher than estimations for bulk materials, this is common for thin films and nanostructures. In particular, high resistances of DVD-based samples may be related to

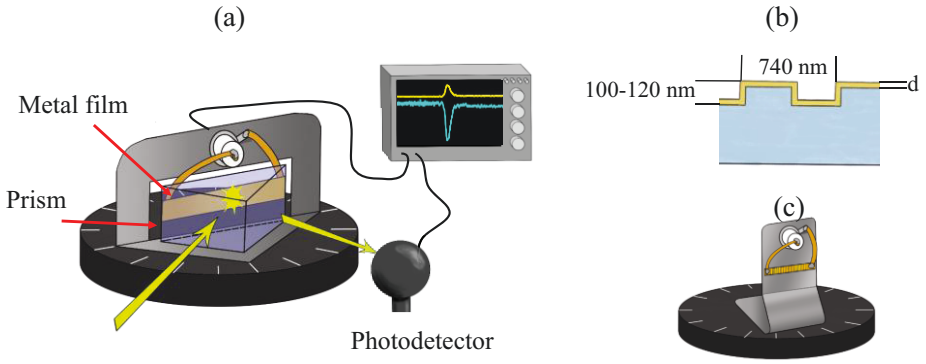

Figure 4. (a) Setup; (b) Schematics of the DVD-based sample; (c) holder for the DVD-based sample.

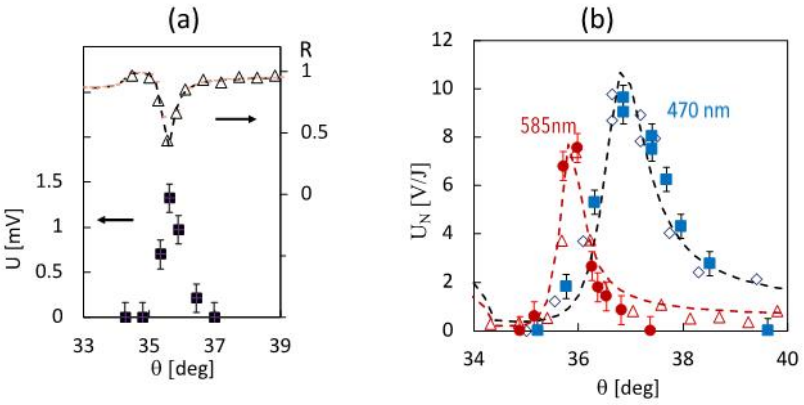

Figure 5. Experiment and fitting in silver. (a) Photovoltage magnitude (closed symbols) and reflectance (open symbols are experiment, dashed trace is predictions [35]) at λ~ 632 nm; (b) photovoltages normalized to incident pulse energy (closed symbols) and fitting with losses estimated from experimental (open symbols) and theoretical (dashed trace) reflectance, at λ = 585 nm and 470 nm as indicated.

significant variations in film thickness along the profile (vertical walls may be much thinner than horizontal stages).

Special care is taken on mounting the samples to ensure good electrical connections. The samples under study are mounted to a steel support system containing a coaxial BNC connector (see figure 4). This allows for a stable connection to the sample without putting physical stresses on the sample when the angle of incidence is changed. The grating samples, being mounted vertically, are secured to a microscope slide with double sided tape to ensure a perfectly flat mount; the slide is then mounted to the steel support system with the same double-sided tape. To accommodate the prism-based systems, a series of tabs are built into the structure to hold the prism in place, eschewing the need for adhesives to secure it. In either case, the entire structure is then bolted to a rotating stage. Copper tape is soldered to the connections on the BNC connector and attached to the sample using a binary epoxy impregnated with silver nanoparticles.

In the experiment, the sample is illuminated with laser pulses with a duration of 10 ns, energy E_{pulse} = 0.1-0.3 mJ per pulse and a wavelength of λ = 410 nm -750 nm using an Optical Parametric Oscillator (OPO) and a 1.06 micron Nd: YAG laser. The photovoltage signal is recorded with a 2 GHz Tektronix Digital Oscilloscope (at 50 W internal resistance). Reflected light intensity is collected at the same time, with an integrating sphere and a photodetector.

Results

A typical angular dependence of the photovoltage observed in our flat films in the Kretschmann geometry is shown in figure 5 (a). The photovoltage has a maximum at the angle corresponding to the excitation of a SPP, which is seen from the reflectance dip. This is expected and correlates well with multiple previous studies. Our current goal is the estimation of the magnitude of the photovoltage response to light illumination in various samples and at various wavelengths. We normalize the photovoltage to the experimentally measured pulse energy. In our experimental conditions (illuminated area of 3x 4 mm and pulse duration of 10 ns) an energy of 0.1 mJ per pulse corresponds to a power of 0.83 MW/mm^2.

First, let us assume that at the same illumination conditions and in the same material, the photovoltage signal linearly depends on the light intensity; this was observed in previous studies [18]. Since in our samples we do not have perfect coupling of incoming light and SPPs and only a part of the pulse energy is absorbed, we use the following procedure in our estimations, depicted in figure 5 (b). Neglecting transmission and reflection from glass, the pulse energy absorbed at a particular incidence angle, θ, is estimated from the reflectance $R(\theta)$ as $(1-R/R_0)E_{pulse}$ where R_0 is the reflectance taken far from the resonance. In figure 5 (b) we plot together the experimental photovoltage normalized to the incoming pulse energy, U_N, (closed symbols) and $(1- R/R_0)$ multiplied to a fitting parameter a. Open symbols correspond to experimental measurements of the reflected intensity, and the dashed curve is from the theoretical reflectance [35] estimated for this geometry. As one can see, the angular dependence of the photovoltage follows well the angular dependence of the losses. The fitting parameter a characterizes the photovoltage response per absorbed energy.

The results obtained in various materials are shown in figure 6. We use the fitting approach discussed above to estimate the photovoltage per pulse energy in the flat films. In flat silver

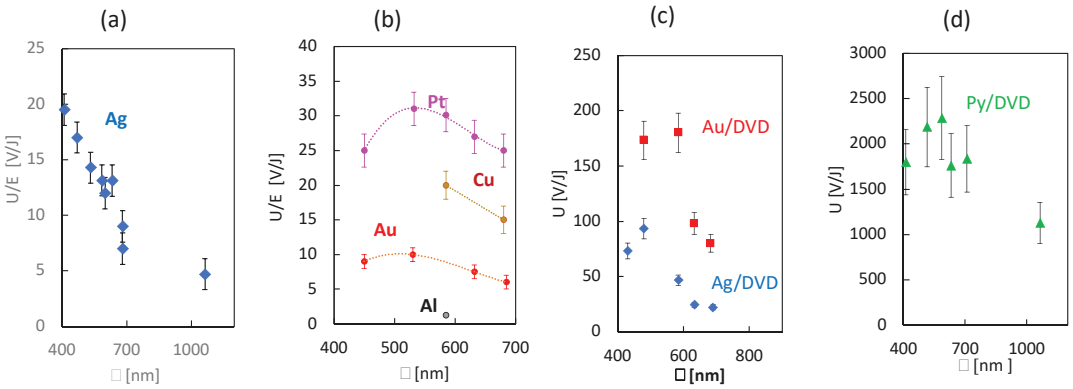

Figure 6. Photovoltage normalized to absorbed pulse energy in (a,b) flat films; (c) and (d) DVD-based gratings. Materials are indicated with color. Dotted trances are guide for eye.

films (figure 6 (a)), the photovoltage normalized to absorbed power steeply decreases upon increase in the wavelength. Similar tendency is observed in other materials as well, with a broad maximum of the photovoltage observed at shorter wavelengths (figure 6 (b)). The magnitude significantly varies depending on the material, showing the smallest values in aluminum and highest in platinum. The results obtained in DVD-based silver and gold gratings (Ag/DVD and Au/DVD) are plotted in figure 6 (c), and the results obtained in permalloy gratings (Py/DVD) are shown in figure 6(d). Note that optical and photovoltage behavior in such profile-modulated systems is complicated. These systems have multiple plasmonic resonances and may demonstrate a sharp switching in the signal polarity with small variations in incidence angle [24]. For a rough estimate of the SPP-related response in gratings, we consider signals with the polarity corresponding to an electron drift in the direction of SPP propagation and assume the efficiency of the SPP excitation to be 30% in silver gratings, 25% in gold gratings and 20% in permalloy gratings based on our previous experiments [24, 32]. The spectral behaviour of *U/E* in gratings shows a maximum at short wavelengths (with the position different for different materials) and a decrease with the increase in the wavelength. In comparison with the flat gold and silver films, the magnitude of the response in the gold and silver gratings is higher by an order of magnitude. The magnitude of the response greatly varies as the function of the material and structure. The Py/DVD structure shows the highest response in voltage per absorbed pulse energy. It exceeds the lowest response, which is observed in flat aluminum films by more than three orders in magnitude.

Discussion

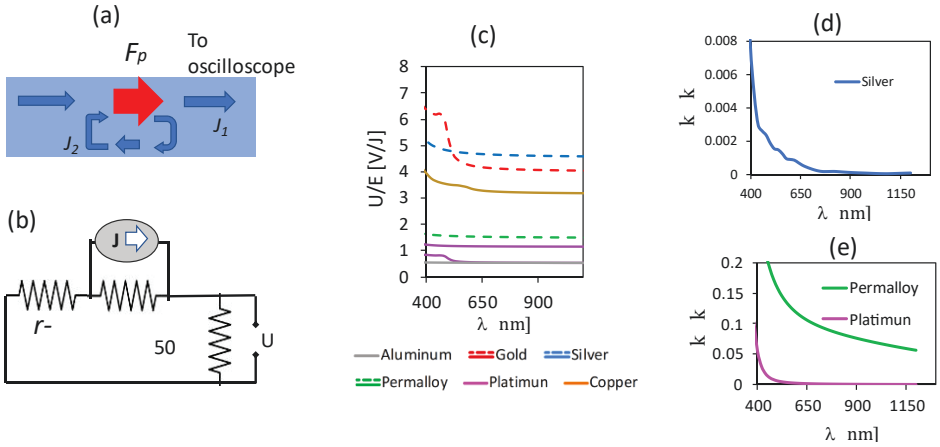

Figure 7. (a) Photoinduced effective force (red arrow) and current flow (blue arrows) in the film cross-section; (b) Equivalent electrical circuit, featuring the DC current source; (c) Predictions of the plasmonic pressure mechanism, solid traces are flat films, dashed traces are gratings. (d) and (e) are theoretical estimations of k''/k_0.

Thus, experiments show: (i) the presence of plasmon-related photovoltages in all materials tested; (ii) strong variations in the magnitude of the signal dependent upon the material; (iii) enhanced values in gratings compared to flat films; and (iv) a general decrease in the magnitude upon an increase in the wavelength with a broad maximum in some samples (with the position dependent on material and structure (flat films or gratings)).

Let us now compare the results with the theoretical predictions discussed above by making some assumptions about an equivalent electrical circuit. The action of the pressure force can be considered as a current source. In the DC regime, the photoinduced electromotive force induces the electric current with the current density [27] in the illuminated spot,

$$j = nev = ne\,\frac{f_p}{m}\tau, \qquad (6)$$

where v is the average electron drift velocity, m is the electron mass, τ is the momentum relaxation time, and f_p is the volume density of the pressure force. In the terms of the pressure force per area, F_p, acting in the thin film, the total photoinduced current in the strip with the width a can be found as

$$J = ane\,\frac{F_p}{m}\tau. \qquad (7)$$

Let us also take into account a possible shortcut due to the low resistance of the illuminated spot (figure 7 (a)), and consider the equivalent circuit shown in figure 7 (b). The voltage measured with the oscilloscope with the internal resistance r_o = 50 W can be found as

$$U = J * \frac{r_i\, r_0}{r + r_0} = a\,ne\,\frac{F_p}{m}\tau\,\frac{r_i\, r_0}{r + r_0}, \qquad (8)$$

where r_i is the resistance of the illuminated film, and r is the total resistance of the film, electrical contacts and wires. For rough estimations for voltages expected in our samples, we neglect the resistance of the wires and contacts, assume $r_i = r/4$ (corresponding to the relative length of the illuminated spot), and use resistances r from Table 1. The width, a = 3 mm, and τ is the Drude relaxation time. As upper limits we assume τ = 4*10^{-14} s in silver, 3*10^{-14} s in gold, 0.8*10^{-14} s in aluminum, 2.7*10^{-14} s in copper [36], and 1*10^{-14} s in platinum and permalloy.

The estimations are shown in figure 7 (c). The gold and silver gratings (showed with dashed traces) are expected to show higher photovoltage than flat gold and silver films. This is observed in the experiment, figure 6, where the photovoltage in Au and Ag gratings is significantly higher than that in the flat silver and gold samples. Thus, the order of magnitude enhancement of the photovoltages in nanostructured samples can be simply related to higher resistances of those samples.

However, the experimental observations differ from the theoretical predictions. The experimental magnitudes are significantly higher than predicted, in particular in permalloy systems. Experimental spectral behavior does not correspond to the predictions either: the experiments show a clear decrease with an increase in the wavelength.

The fact, that the photovoltages are observed and demonstrate similar spectral dependences in all metals tested, may indicate that the mechanism is common for all of them and likely does not involve inter-band transitions. We should note that our estimations are made using a number of assumptions: (i) Considering perfectly flat films (neglecting possible roughness); (ii) Assuming bulk permittivities for metals (while in thin films, effective values can be different), and (iii) Using Drude time constants for the momentum relaxation (they can be different for hot electrons). We believe that the factors such as roughness and dynamics of hot electrons can play a significant role, and should be considered for further development of the theoretical approach. In addition, the current theoretical approach [26] is very general and does not consider particular mechanisms of light-matter interaction. The Landau damping mechanism [37] is a well-known mechanism for the interaction of light and electron plasma. In a relativistic plasma, it creates a flux of electrons by trapping them in a propagating wave. In metals, such trapping is not expected since Fermi velocities are significantly lower than the speed of light. However, this mechanism plays a role in the decay of plasmon waves [38]. The decay of the SPP along the propagation path is characterized by the imaginary part of the SPP k-vector, k''. In figure 7 (d, e), we plot k''/k_0 for different metals; surprisingly, both the spectral behavior and variation in the dependence on metal correspond to the experimental observations for *U/E* (see figure 6).

Conclusion

The plasmon-related voltages are studied experimentally and theoretically as they depend on material, structure, and wavelength. Experiments show that the photoresponses exhibit a general decrease with an increase in the wavelength and strongly vary depending upon the material. The experimental results will be used to further develop a theoretical description of the plasmon drag effect.

Acknowledgements

The authors would like to thank the following grants for the funding that made this work possible.

NSF 1830886, NSF 2112595, AFOSR FA9550-18-0417, and DOE NNSA DE-NA0004007

References

[1] Noginov, M., 2009. *Metamaterials: fundamentals and applications II*. Bellingham, Wash: SPIE.

[2] Brongersma, M.L. and Shalaev, V.M., 2010. The case for plasmonics. *Science*, 328(5977), pp.440-441.

[3] Tong, X.C., 2018. *Functional metamaterials and metadevices*. Bolingbrook, IL: Springer.

[4] Wachsmann-Hogiu, S., Smith, Z.J. and Kahraman, M., 2019. *Plasmonic Technologies for Bioanalytical Applications. Frontiers in Chemistry*, p.865.

[5] Liu, Y. and Zhang, X., 2011. Metamaterials: a new frontier of science and technology. *Chemical Society Reviews*, 40(5), pp.2494-2507.

[6] Ziolkowski, R.W. and Kipple, A.D., 2003. Causality and double-negative metamaterials. *Physical Review E*, 68(2), p.026615.

[7] Schuller, J.A., Barnard, E.S., Cai, W., Jun, Y.C., White, J.S. and Brongersma, M.L., 2010. Plasmonics for extreme light concentration and manipulation. *Nature materials*, 9(3), pp.193-204.

[8] Zayats, A.V., Smolyaninov, I.I. and Maradudin, A.A., 2005. Nano-optics of surface plasmon polaritons. *Physics reports*, 408(3-4), pp.131-314.

[9] Shaltout, A.M., Shalaev, V.M. and Brongersma, M.L., 2019. Spatiotemporal light control with active metasurfaces. *Science*, 364(6441), p.eaat3100.

[10] Noginov, M.A., Zhu, G., Bahoura, M., Small, C.E., Davison, C., Adegoke, J., Drachev, V.P., Nyga, P. and Shalaev, V.M., 2006. Enhancement of spontaneous and stimulated emission of a rhodamine 6G dye by an Ag aggregate. *Physical review B*, 74(18), p.184203.

[11] Tumkur, T.U., Kitur, J.K., Bonner, C.E., Poddubny, A.N., Narimanov, E.E. and Noginov, M.A., 2015. Control of Förster energy transfer in the vicinity of metallic surfaces and hyperbolic metamaterials. *Faraday discussions*, 178, pp.395-412.

[12] Ueno, K. and Misawa, H., 2013. Surface plasmon-enhanced photochemical reactions. *Journal of Photochemistry and Photobiology C: Photochemistry Reviews*, 15, pp.31-52.

[13] Mukherjee, S., Libisch, F., Large, N., Neumann, O., Brown, L.V., Cheng, J., Lassiter, J.B., Carter, E.A., Nordlander, P. and Halas, N.J., 2013. Hot electrons do the impossible: plasmon-induced dissociation of H2 on Au. *Nano letters*, 13(1), pp.240-247.

[14] Brongersma, M.L., Halas, N.J. and Nordlander, P., 2015. Plasmon-induced hot carrier science and technology. *Nature nanotechnology*, 10(1), pp.25-34.

[15] Vengurlekar, A.S. and Ishihara, T., 2005. Surface plasmon enhanced photon drag in metal films. *Applied Physics Letters*, 87(9), p.091118.

[16] Noginova, N., Yakim, A.V., Soimo, J., Gu, L. and Noginov, M.A., 2011. Light-to-current and current-to-light coupling in plasmonic systems. *Physical Review B*, 84(3), p.035447.

[17] Kurosawa, H. and Ishihara, T., 2012. Surface plasmon drag effect in a dielectrically modulated metallic thin film. *Optics Express*, 20(2), pp.1561-1574.

[18] Noginova, N., Rono, V., Bezares, F.J. and Caldwell, J.D., 2013. Plasmon drag effect in metal nanostructures. *New Journal of Physics*, 15(11), p.113061.

[19] Kurosawa, H., Ishihara, T., Ikeda, N., Tsuya, D., Ochiai, M. and Sugimoto, Y., 2012. Optical rectification effect due to surface plasmon polaritons at normal incidence in a nondiffraction regime. *Optics letters*, 37(14), pp.2793-2795.

[20] Akbari, M., Onoda, M. and Ishihara, T., 2015. Photo-induced voltage in nano-porous gold thin film. *Optics express*, 23(2), pp.823-832.

[21] Sheldon, M.T., Van de Groep, J., Brown, A.M., Polman, A. and Atwater, H.A., 2014. Plasmoelectric potentials in metal nanostructures. *Science*, 346(6211), pp.828-831.

[22] van de Groep, J., Sheldon, M.T., Atwater, H.A. and Polman, A., 2016. Thermodynamic theory of the plasmoelectric effect. *Scientific reports*, 6(1), pp.1-12.

[23] Noginova, N., LePain, M,. Rono, V., Mashhadi, S. , Hussain, R., and Durach, M., "Plasmonic pressure in profile-modulated and rough surfaces," *New J. Phys*. 18, 093036 (2016).

[24] Ronurpraful,T., Keene, D., and Noginova, N., "Plasmon drag effect with sharp polarity switching," *New J. Phys*. 22, 043002 (2020).

[25] Ronurpraful, T., Jerop, N., Koech, A., Thompson, K., and Noginova, N, "Extreme sensitivity of plasmon drag to surface modification," *J. Phys. D* 54, 035307 (2021).

[26] Durach, M., Rusina, A., and Stockman, M. I., "Giant surface-plasmon induced drag effect in metal nanowires," *Phys. Rev. Lett*. 103, 186801 (2009).

[27] Durach, M. and Noginova, N., "On the nature of the plasmon drag effect," *Phys. Rev. B* 93, 161406 (2016).

[28] Kurosawa, H., Ohno, S., and Nakayama, K., "Theory of the optical rectification effect in metallic thin films with periodic modulation," *Phys. Rev. A* 95, 033844 (2017).

[29] Durach, M. and Noginova, N., "Spin angular momentum transfer and plasmogalvanic phenomena," *Phys. Rev. B* 96, 195411 (2017).

[30] Strait, J. H., Holland, G., Zhu, W., Zhang, C. , Ilic, B. R., Agrawal, A., Pacifici, D., and Lezec, H. J., "Revisiting the photon-drag effect in metal films," *Phys. Rev. Lett.* 123, 053903 (2019).

[31] Mikheev, G. M., Saushin, A. S., Styapshin, V. M., and Svirko, Y. P.,"Interplay of the photon drag and the surface photogalvanic effects in the metal-semiconductor nanocomposite," *Sci. Rep.* 8, 8644 (2018).

[32] Shahabuddin, M., Keene, D., Durach, M. , Posvyanskii, V.V., Atsarkin, V. A., Noginova, N., "Magnetically

dependent plasmon drag in permalloy structures," *JOSA B* 38, 2012 (2021).

[33] Kretschmann, E. and Raether, H., "Radiative Decay of Non Radiative Surface Plasmons Excited by Light," *Zeitschrift für Naturforschung_A*, vol. 23, no. 12, pp. 2135–2136, 1968.

[34] https://refractiveindex.info/

[35] Raether H., *Surface Plasmons on Smooth and Rough Surfaces and on Gratings*, Springer, 1988.

[36] Ashcroft, N., Mermin, N.D., *Solid State Physics*, New York: Saunders College Publishing, 1976.

[37] Landau, L D., Pitaevskii, L.P., Lifshitz, E.M., *Electrodynamics of Continuous Media*, Vol. 8. 2d Edition. Butterworth-Heinemann 1984.

[38] Shahbazyan, T. V. ,"Landau damping of surface plasmons in metal nanostructures," *Phys. Rev. B* 94, 235431 (2016).